Utilization of Permanent Magnet Synchronous Motors in Industrial Robots

Jan Staszak, Krzysztof Ludwinek, Zbigniew Gawęcki,
Jarosław Kurkiewicz, Tomasz Bekier
Division of Power Engineering Electronics, Electrical Machines and Drives
Kielce University of Technology
Kielce, Poland
{j.staszak, k.ludwinek, z.gawecki, jkurkiewicz, tbekier}@tu.kielce.pl

Marek Jaśkiewicz
Division of Automotive Vehicles and Transportation
Kielce University of Technology
Kielce, Poland
m.jaskiewicz@tu.kielce.pl

***Abstract* — The paper presents results of research concerning the basis of utilization of PMSMs in industrial robots. A mathematical model of PMSM is described. Identification of PMSM's parameters is performed as well as an analysis of simulation and experimental investigation results of transients and steady states of electrical and mechanical quantities is presented.**

Keywords — PMSM, industrial robot, parameter identification

I. INTRODUCTION

Permanent magnet motors can be divided into two categories:

- with trapezoidally shaped Electromotive force (EMF) and approximately rectangular current waveform (structure known as brushless DC motor (BLDC) with permanent magnets and requires rotor's position detection every 60° of electrical angle) [1],
- with sinusoidal EMF and near-sinusoidal current (structure known as permanent magnet synchronous motor (PMSM) which requires continuous detection of rotor's position) [2-7].

In theoretical considerations it is commonly assumed that voltage and current waveforms, which determine rotational speed and electromagnetic torque for both BLDC motors and PMSMs, do not generate torque ripple [1]. Such idealized waveforms of EMF and current for BLDC motor and PMSM are presented in Fig. 1 [2].

However, the occurrence of torque ripple and speed ripple decides on practicality of BLDC and PMSMs application in, for example, servomotors. Torque ripple and rotational speed pulsations are determined mainly by [1, 2]:

- occurrence of stator and rotor slotting,
- distortion of the stator current and its limited rise time,
- stator's winding inductance distortion (as a function of rotor's angle of rotation),
- PM's magnetic field distortion.

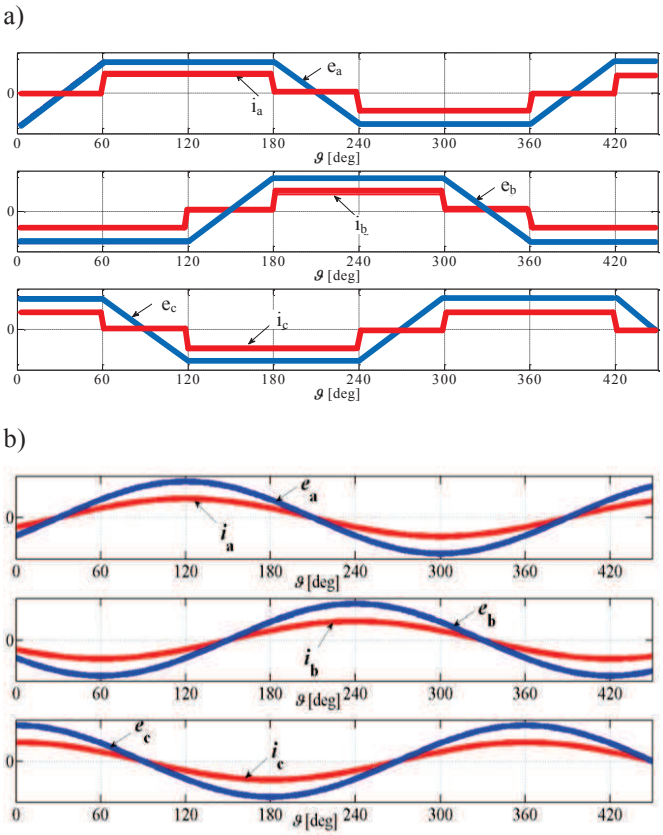

Figure 1. Idealized EMF and current waveforms for a) BLDC, b) PMSM.

In BLDC motors it is much more difficult to achieve short rise times of current, which are required to minimize electromagnetic torque ripple [1]. Registered sample EMF and current waveforms of P_n=120 W BLDC motor are shown in Fig. 2 [1].

Due to significant electromagnetic torque ripple of BLDC motors they are not used in servomotors [2]. Therefore, drive systems requiring both wide range of rotational speed control and precise positioning utilize brushless permanent magnet synchronous motors supplied with sinusoidal current [8,9]. EMF induced in the armature winding due to rotating magnets

978-1-4673-7186-5/15/$31.00 ©2015 IEEE

is sinusoidal thanks to the shape of magnets placed in the rotor and appropriate arrangement of stator's three-phase winding.

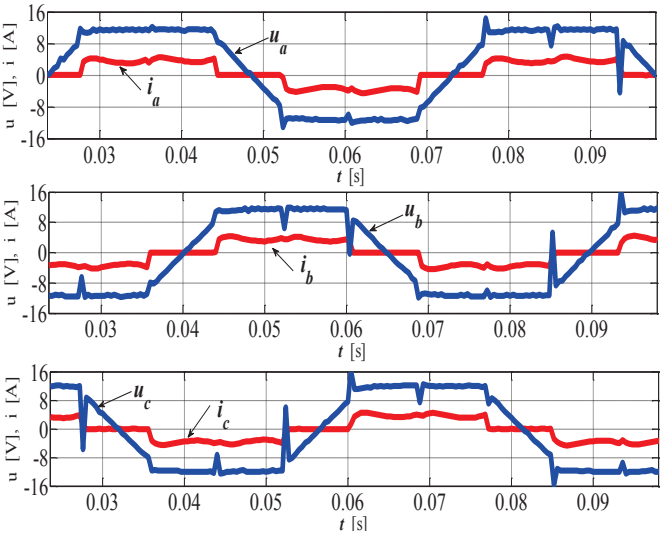

Figure 2. Registered current and EMF waveforms of a BLDC motor.

II. PMSM Mathematical Model

The mathematical model of PMSM employs *dq* rotating reference frame coupled with rotor's flux; as shown in Fig. 3. Axis of the rotor's field overlaps *d* axis [2].

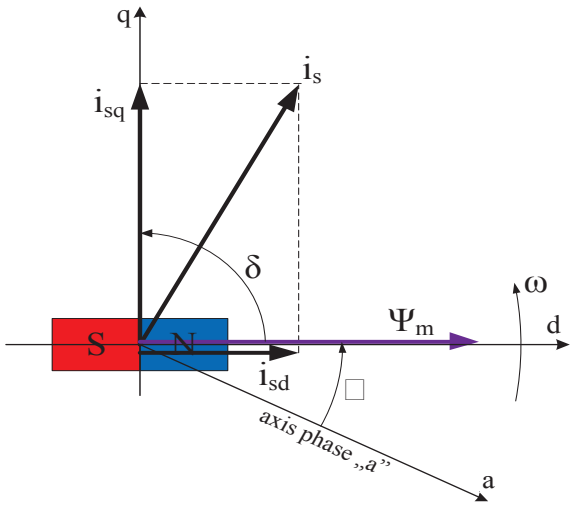

Figure 3. Vector diagram of stator's current and magnets' flux in dq reference frame.

Voltage and flux equations in *dq* reference frame as well as electromagnetic torque equation are expressed as follows [7]:

$$\left.\begin{aligned} u_{sd} &= R_s i_{sd} + \frac{d\Psi_{sd}}{dt} - \omega\Psi_{sq} \\ u_{sq} &= R_s i_{sq} + \frac{d\Psi_{sq}}{dt} + \omega\Psi_{sd} \end{aligned}\right\} \quad (1)$$

$$\left.\begin{aligned} \Psi_{sd} &= L_d i_{sd} + \Psi_m \\ \Psi_{sq} &= L_q i_{sq} \end{aligned}\right\} \quad (2)$$

$$T_e = \frac{3}{2} p_b [\Psi_{sd} i_{sq} - \Psi_{sq} i_{sd}] \quad (3)$$

where: : u_{sd}, u_{sq} – stator's voltage components in d and q axes, i_{sd}, i_q – stator's current components in d and q axes, Ψ_{sd}, Ψ_{sq} – stator linked magnetic flux components in d and q axes, L_{sd}, L_{sq} – stator's winding inductances in d and q axes, ω – electrical angular velocity of the rotor, p_b – pole pair count, T_e – electromagnetic torque.

By substituting flux equations (2) in (1) and (3) the following result is obtained:

$$\left.\begin{aligned} u_d &= R_s i_{sd} + L_d \frac{di_{sd}}{dt} - \omega L_q i_{sq} \\ u_{sq} &= R_s i_{sq} + L_q \frac{di_{sq}}{dt} + \omega L_d i_{sd} + \omega\Psi_m \end{aligned}\right\} \quad (4)$$

$$T_e = \frac{3}{2} p_b [\Psi_m i_{sq} + (L_d - L_q) i_{sd} i_{sq}] \quad (5)$$

In order to mathematically describe PMSM dynamics the voltage equations (4) and electromagnetic torque expression (5) need to be supplemented by the following equation of motion:

$$J\frac{d\Omega}{dt} + D\Omega + T_h = T_e \quad (6)$$

where: J – moment of inertia, D – viscous friction factor, T_h – load torque, Ω - mechanical angular velocity, wherein $\omega = p_b\Omega$.

By utilizing field-oriented control it is possible to achieve a maximum electromagnetic torque for a given PMSM's stator current [10]. Under such circumstances the stator current in *d* axis i_{sd} is equal to zero. Then (4) and (5) take the following form:

$$\left.\begin{aligned} u_{sd} &= -\omega L_q i_{sq} \\ u_{sq} &= R_s i_{sq} + L_q \frac{di_{sq}}{dt} + \omega\Psi_m \end{aligned}\right\} \quad (7)$$

$$T_e = \frac{3}{2} p_b \Psi_m i_{sq} \quad (8)$$

It should be noted that by transforming the equations to the rotating *dq* reference frame the electromagnetic torque of PMSM becomes linearly dependent on the stator current in a similar fashion to externally excited DC motor.

Fig. 4 presents a structural diagram of a PMSM as a control object. This diagram is analogous to that of a DC motor as long as the condition of zero stator current in d axis i_{sd}=0 is maintained.

Fig. 5 shows one of possible control block diagrams of a PMSM. Such motors are characterized by sinusoidal stator phase currents and armature induced voltages [2, 7].

In order to obtain a constant electromagnetic torque at a given armature current it is necessary to continuously measure the precise angle of the rotor's position, which, in turn, makes it possible to utilize vector control of the inverter. In the system shown in Fig. 5 a resolver is used to detect rotor's position. The output signal from the speed controller R_ω constitutes the requested current value i_{sqref}. Given a known rotor's position ϑ from the resolver it is possible for current components in the *dq* rotating reference frame to be further transformed in *dq/abc* block to phase currents i_{saref}, i_{sbref}, i_{scref}. These currents are compared in a hysteresis regulator RH to measured phase currents i_{sa}, i_{sb}, i_{sc} and, as a result, logic signals S_a, S_b and S_c are generated which control inverter's (INV) transistors.

III. PMSM'S PARAMETER IDENTIFICTATION

L_d and L_q inductances are most frequently obtained experimentally [3, 4, 9]. L_d and L_q of the PMSM were acquired through the use of DC current rise method in the measuring system shown in Fig. 6. The process of DC current rise is initialized by closing switch B. In the process of L_d and L_q identification it was assumed that i_s stator current rises mono-exponentially and can be expressed as:

$$i_s = I_{s0}\left(1 - e^{-\frac{t}{T_s}}\right) \tag{9}$$

where: I_{s0} - steady state value of the measurement current, T_s - measuring system time constant

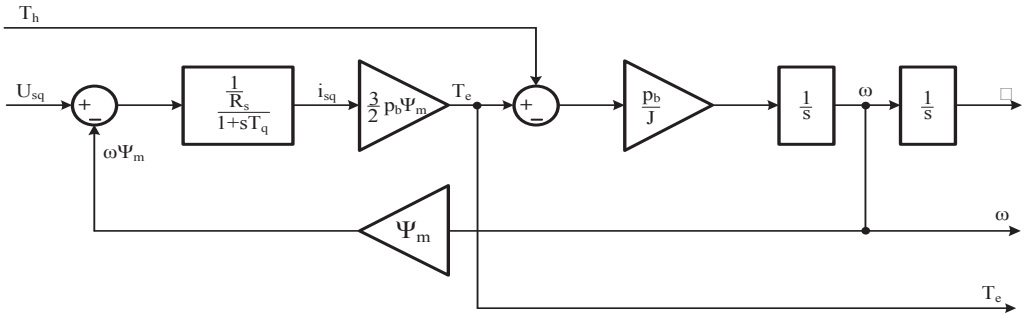

Figure 4. Structural block diagram of a permanent magnet synchronous motor.

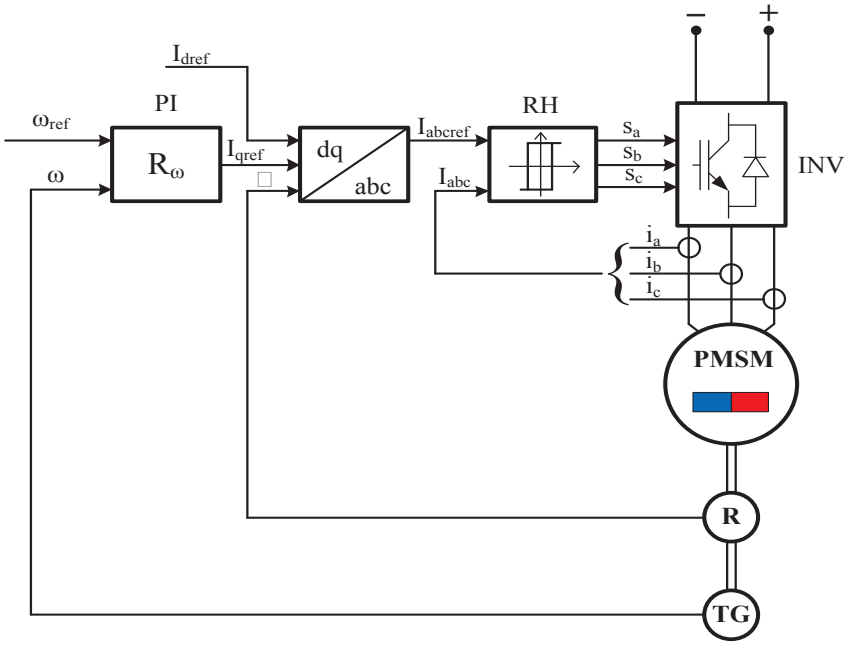

Figure 5. Control block diagram of a permanent magnet synchronous motor.

978-1-4673-7186-5/15/$31.00 ©2015 IEEE

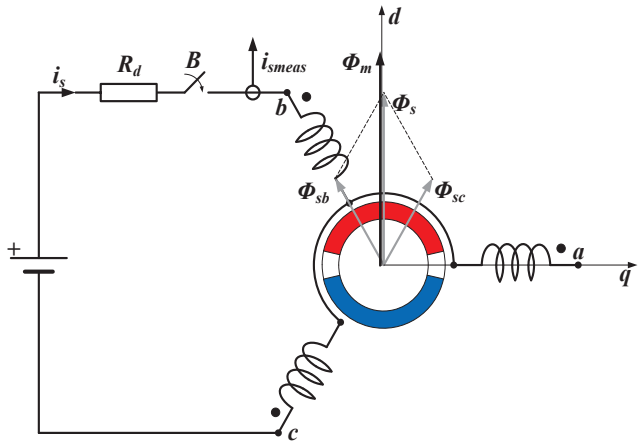

Figure 6. Diagram of the measuring system used to register DC current rise in the stator.

Steady state component of I_{s0} current and rise time constant T_s were determined based on the registered waveform of the stator current rise in the measuring circuit (Fig. 6). The sought values of the vector of coefficients x = [I_{s0} T_s] were found using Levenberg-Marquardt method minimizing mean squared error:

$$\varepsilon = \sum_{k=1}^{N} \left[i_s(t_k) - i_{smes}(t_k, \mathbf{x}) \right]^2 \qquad (10)$$

where: $i_s(t_k)$, $i_{smes}(t_k,\mathbf{x})$ – current rise waveforms obtained experimentally and by approximation, N – sample count.

Computations were carried out in Matlab environment. Fig. 7 presents both registered stator current rise and one derived from the approximation.

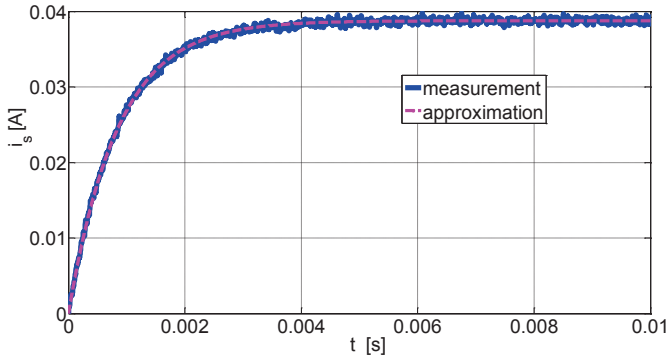

Figure 7. Registered and approximated current rise waveforms in stator's windings.

L_d inductance of armature winding is derived from the following expression:

$$L_d = RT_s \qquad (10)$$

where: T_s – current rise time constant in the measuring circuit, R – single phase resistance of the armature winding.

Due to the symmetry of the armature's magnetic circuit along d and q axes the inductance $L_q = L_d$. Single phase resistance of the armature winding is equal to half the measuring circuit resistance $R = R_s + 0.5R_d$, where R_d is an additional resistance of the measuring circuit and R_s is the armature resistance. Remaining electromechanical parameters of the examined PMSM, i.e. magnets' flux Ψ_m and moment of inertia J, were obtained from manufacturer's datasheet [12]. The values of electrical and mechanical parameters used in the computation are presented in Table I.

TABLE I. ELECTRICAL AND MECHANICAL PARAMETERS

Symbol	Name	Value	Unit
R_s	Armature resistance	11.9	Ω
L_d	d axis inductance	13.26	mH
p_b	Number of pole pairs	4	-
k_T	Torque constant	0.168	Nm/A
J	Moment of inertia	0.012	kgcm2

IV. SIMULATION STUDY

PMSM's simulation study has been carried out in Matlab/Simulink environment. Fig. 8 presents waveforms of armature phase currents i_a, i_b and i_c as well as current components in d and q axes of the examined motor. In the course of the simulation friction has been neglected and rated load has been applied after 0.02s. Those and following results were all obtained using block diagram shown in Fig. 9.

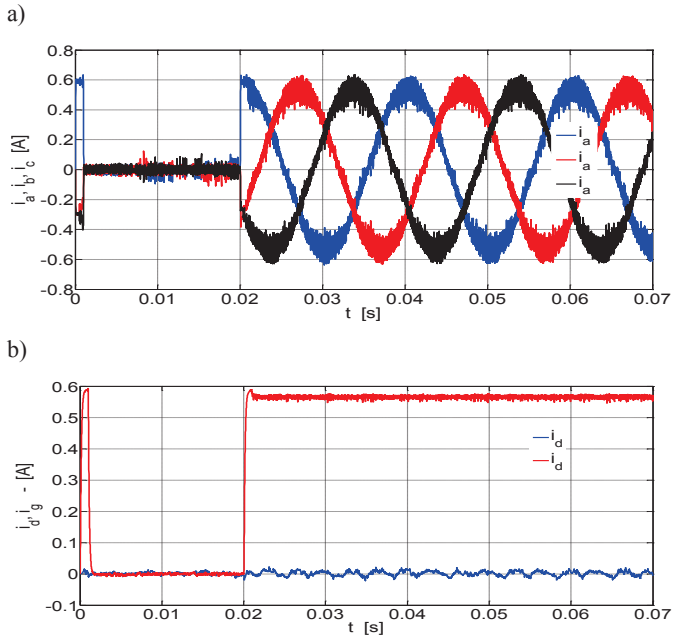

Figure 8. Waveforms of a) armature phase currents i_a, i_b, i_c b) current components in d and q axes.

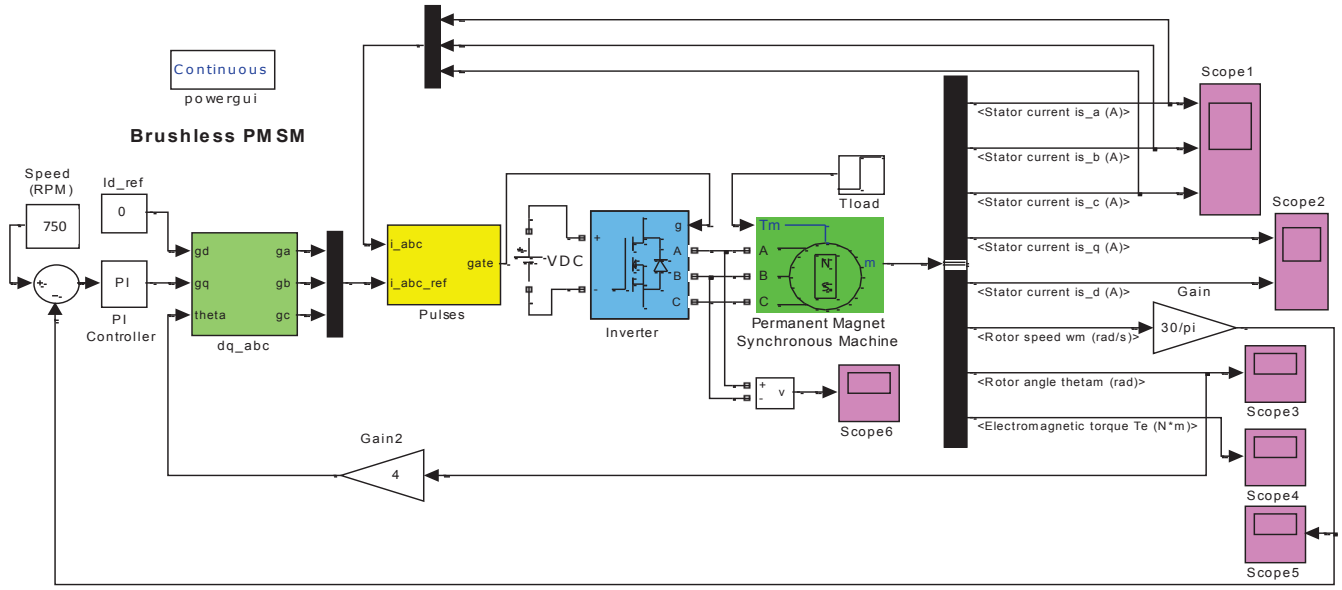

Figure 9. Permanent magnet synchronous motor block diagram used for simulation.

Rotational speed and electromagnetic torque waveforms are shown in Fig. 10 and Fig. 11 respectively.

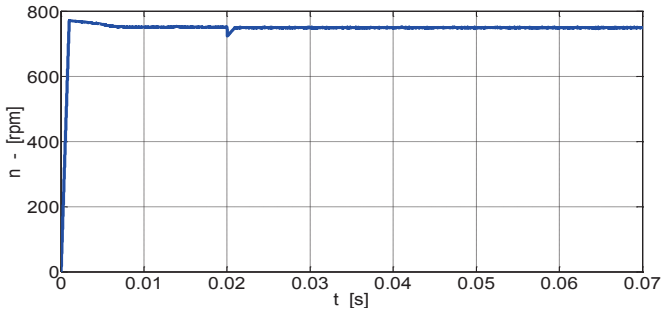

Figure 10. Rotational speed vs time graph.

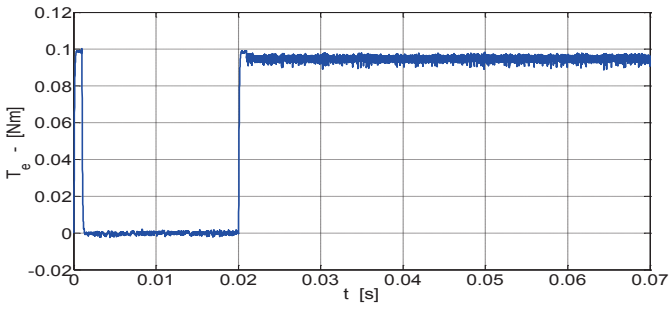

Figure 11. Electromagnetic torque waveform.

V. Experimental Study

Experimental investigation concerned the PMSM of identical to simulation rating. Motors of this particular type rated at 30W are mounted on Yamaha's SCARA robot Y, Z and R axes. The presented robot is being controlled by means of the Ethernet interface, which, in the face of broadband network commonness, is becoming increasingly popular for remote control and monitoring of electrical machines even across the Internet [13]. Appropriate Ethernet communication module configuration connected with Omron PLCs of type CJ and CS is presented in [14]. Measurement stand used to investigate PMSMs is shown in Fig. 12.

a)

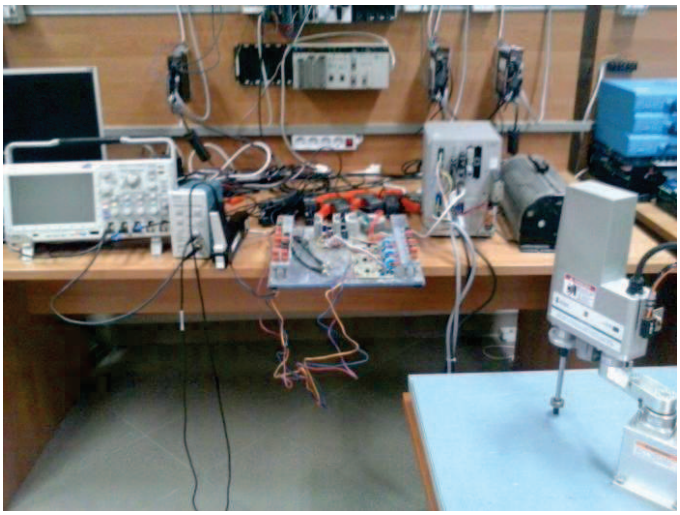

978-1-4673-7186-5/15/$31.00 ©2015 IEEE

b)

c)

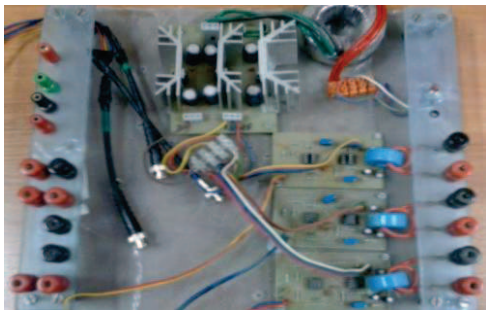

Figure 12. Overview of: a) measurement stand used to investigate PMSMs and SCARA robot, b) robot's arm powered by investigated PMSMs, c) current transducers.

Presented measurement stand consists of:

- SCARA robot central unit and manipulator arm,
- Modular CS1D PLC equipped with analog and digital input/output modules and communication modules utilizing Ethernet, Profibus and Devicenet standards,
- Digital storage oscilloscope Tektronix MSO3014,
- Current probes set including A621, A622 and TCP303 together with TCPA300 amplifier,
- Current transducers set constructed by one of the authors [15] based on [16 - 18],
- Additional resistance unit R_d and 12 V, 18 Ah gel battery.

Fig. 13 presents registered phase current waveforms of the investigated PMSM.

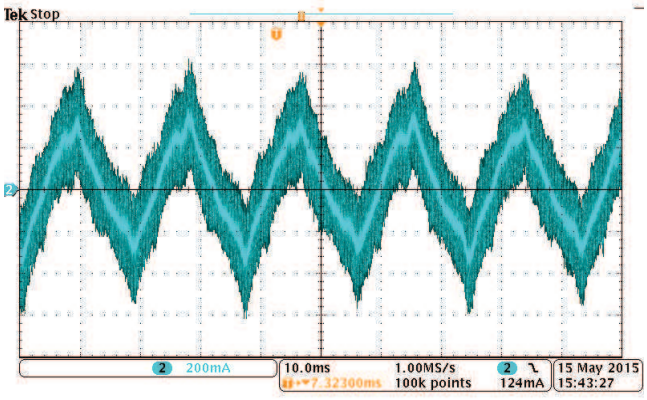

Figure 13. Registered current waveform of the examined motor.

VI. Conclusion

The article presents a mathematical model of permanent magnet synchronous motor rated at 30W, which is utilized in a positioning system of SCARA robot in X,Y,Z and R axes. Values of inductances in *d* and *q* axes are based on experimental investigation and were used in simulation studies in Matlab/Simulink of currents and electromagnetic torque of the PMSM. Obtained current waveforms and amplitudes are very similar and differences are a result of simulation model simplification.

References

[1] R.Nadolski, K. Ludwinek, J. Staszak, M. Jaśkiewicz, Utilization of BLDC motor in electrical vehicles. Przegląd Elektrotechniczny, Vol. 88, No. 4, 2012. pp. 180-186.

[2] K. Zawirski, Control of Permanent Magnet Synchronous Motor (in Polish), Publishing House of Politechnika Poznańska, Poznań 2005.

[3] A. Soualmi, F. Dubas, D. Dépernet, A. Randrai, Ch. Espanet, Inductances Estimation in the d-q Axis for an Interior Permanent-Magnet Synchronous Machines with Distributed Windings. Journal of Energy and Power Engineering 7 (2013) pp. 1178-1185.

[4] G. H. Lee, W. Choi, B.-H. Lee, J.-W. Jung, J.-P. Hong, Inductance Measurement of Interior Permanent Magnet Synchronous Motor in Stationary Frame of Reference. Journal of Magnetics 16(4), 391-397 (2011). pp. 391-397.

[5] T. Zhaojun, H. Jiahua, Y. Jin, Study on Vector Control Strategy Simulation for Permanent Magnet Synchronous Motor Based on Double Closed Loop. International Journal of Digital Content Technology and its Applications(JDCTA), Vol. 7, No. 3, 2013. pp. 322-332.

[6] P. Mynarek, M. Kowol, Field-circuit analysis of permanent magnet synchronous motors (in Polish). Zeszyty problemowe – Maszyny Elektryczne Nr 100/2013, pp. 73 - 76.

[7] M. M. Kayalvizhi, M. Akilandeswari, Design And Implementation Of Speed Regulator For A PMSM Using Genetic Algorithm. International Journal of Innovative Research in Science, Engineering and Technology, Volume 3, Special Issue 1, February 2014, International Conference on Engineering, Technology and Science-(ICETS'14) On 10th & 11th February. pp. 866-872.

[8] S. Hamacek, M. Bartlomiejczyk, R. Hrbac, S. Misak, V. Styskala, Energy recovery effectiveness in trolleybus transport, Electric Power Systems Research, Vol. 112, 2014, pp. 1-11.

[9] R. Dolecek, O. Cerny, J. Novak, M. Bartlomiejczyk, Interference in Power system for traction drive with PMSM, Przeglad Elektrotechniczny, Vol. 88, No. 9A, 2012, pp. 204-207.

[10] K. Xu, W. Chen, Y. Xu, M. Gao, Z. He, Vector Control for PMSM. Sensors & Transducers, Vol. 170, No. 5, 2014, pp. 227-233.

[11] K. Ludwinek, J. Staszak, Possibility of graphical environment applications for evaluating of equivalent circuit parameters and time constants. Przegląd Elektrotechniczny, Vol. 87, No. 12A. 2011. pp. 195 - 200.

[12] Highly Reliable Servo Motor System (Resolver Type). PDF catalog, http://www.tamagawa-seiki.com/pdf/download/1606n7ej.pdf.

[13] T. Węgiel, M. Sułowicz, D. Borkowski, A Distributed System of Signal Acquisition for Induction Motors Diagnostic, in Proc. of the 6th IEEE SDEMPED'2007, Cracow, 2007, pp. 261–265.

[14] K. Ludwinek, B. Krasuski, M. Osiecki, J. Olejarczyk, Industrial PLC networks configuration with CJ1W-ETN21 and CS1W-ETN21 Ethernet modules (in Polish), Napędy i sterowanie, Nr 6, 2009. s. 32-39.

[15] K. Ludwinek, Measurement of momentary currents by Hall linear sensor. Przegląd Elektrotechniczny, No. 10, 2009. pp. 182-187.

[16] P. Ripka, Electric current sensors: a review, Measurement Science and Technology 2010, Vol. 21 n 11, IOP Publishing Ltd. pp. 1-23.

[17] S. Tumański, Handbook of Magnetic Measurements (CRC Press Taylor & Francis Group, 2011).

[18] http://allegromicro.com/sf/3515/